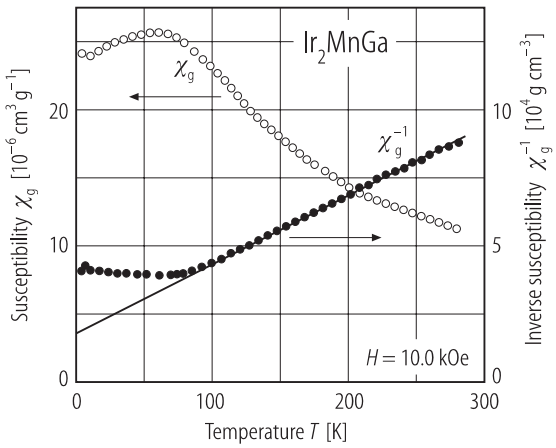

Fig. 120. Temperature dependence of the susceptibility and reciprocal susceptibility of Ir_2MnGa. (T_n = 65 K, Θ = 62 K, p_{eff} = 4.01 μ_B/Mn, a = 6.05 Å) [88Y1].

1.5.5.3.3.3 Paramagnetic

X_2YZ X = 4d, Y = 3d

X = 8A: Pd
Y = 4A: Ti
Z = 3B: Al, Ga, In; 4B: Sn

Pd_2TiZ

These compounds, which have been classified as superweak magnetic, are characterised by small moments and high characteristic temperatures. The bulk susceptibility measurements on Pd_2TiIn suggest antiferromagnetism below ≈ 110 K, but neutron diffraction measurements reveal a structural phase transition at 110 K. Above this temperature the susceptibility is Curie-Weiss, yielding p_{eff} = 4.9 μ_B and Θ = 33.4 K, values surprisingly close to those of Pd_2MnIn. The other compounds in the series have a distinct hysteresis in the magnetisation process.

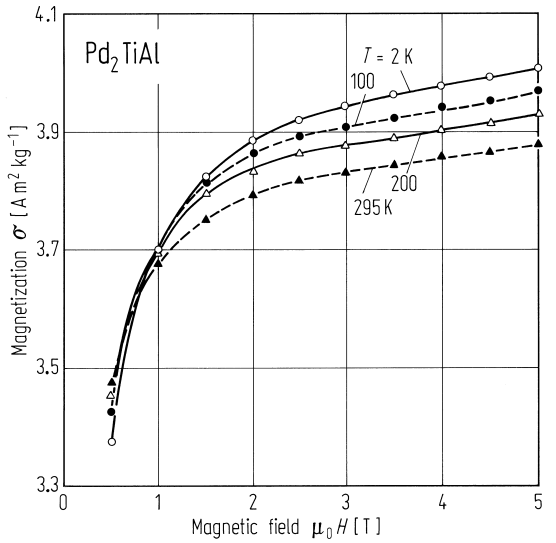

Fig. 121. Isotherms of magnetisation vs. applied field for Pd_2TiAl [94N1].

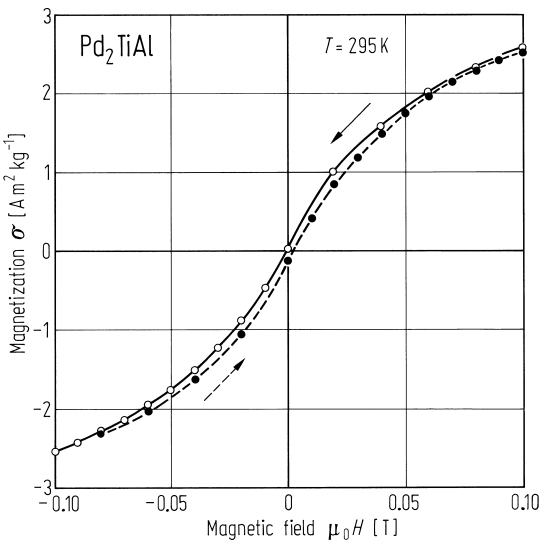

Fig. 122. Magnetic hysteresis of Pd_2TiAl measured at 295 K [94N1].

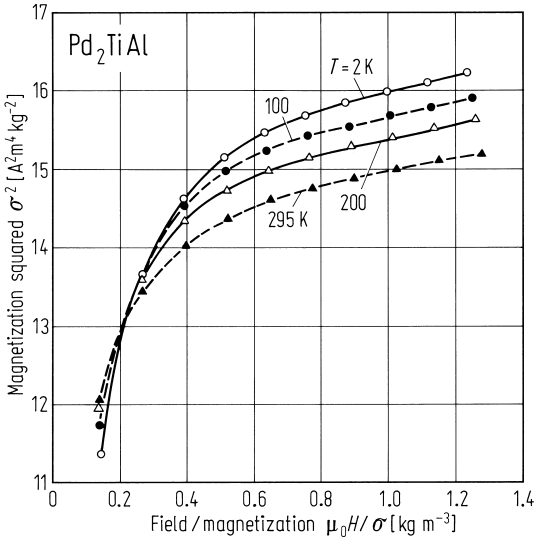

Fig. 123. Arrott plots for Pd_2TiAl [94N1].

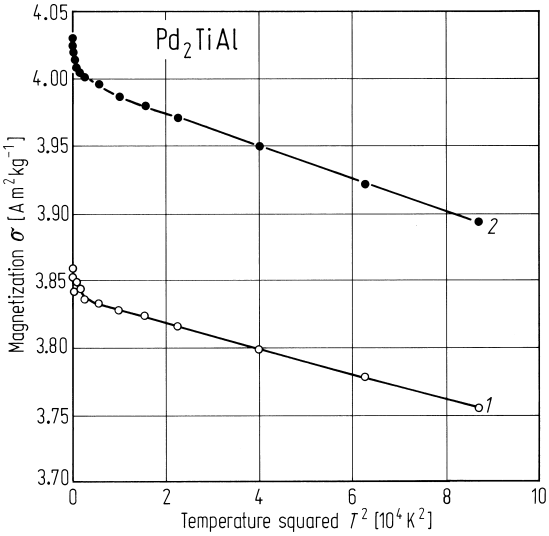

Fig. 124. Thermal variation of the spontaneous magnetisation indicating a T^2 dependence. Curve *1*: spontaneous magnetization, *2*: $\mu_0 H$ = 5 T[94N1].

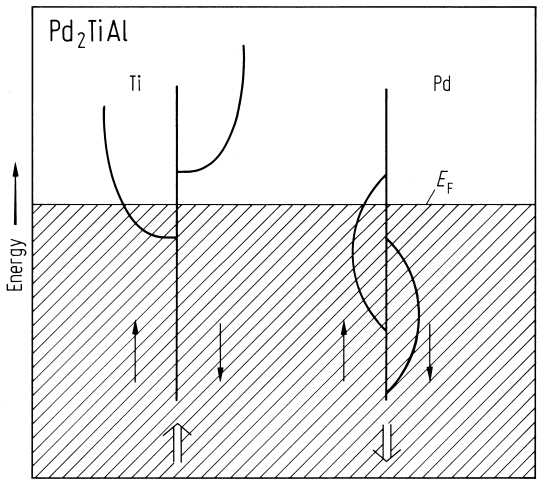

Fig. 125. Schematic representation of the proposed band structure of Pd_2TiAl [94N1].

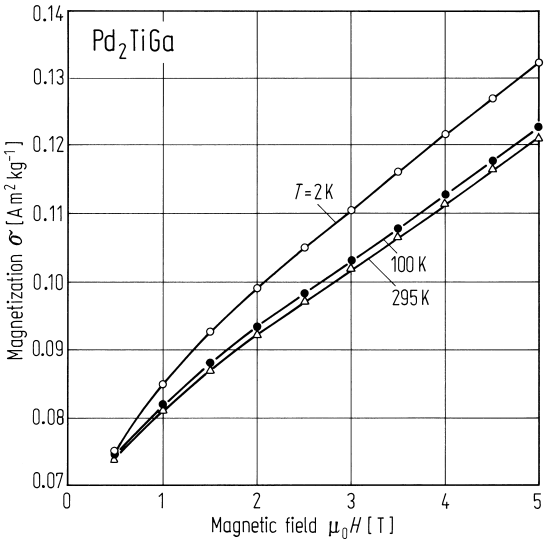

Fig. 126. Magnetisation of Pd_2TiGa between T = 2 K and room temperature [95N2].

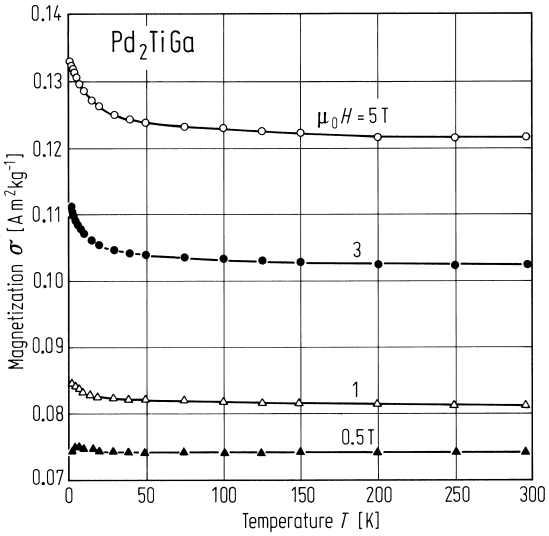

Fig. 127. Plot of the Pd_2TiGa magnetisation as a function of temperature for applied magnetic fields between 0.5 and up to 5 T. Note the suppression of the zero on the y axis [95N2].

Table 25. Summary of the principal properties of Pd_2TiIn compared with those for the related compound Pd_2MnIn; the value for the Néel temperature of Pd_2TiIn was estimated from the broad susceptibility anomaly [93N2].

	a [Å]	T_N [K]	Θ [K]	p_{eff} [μ_B]
Pd_2TiIn	6.365	≈ 110	33.4	4.9
Pd_2MnIn	6.373	143	52	4.9

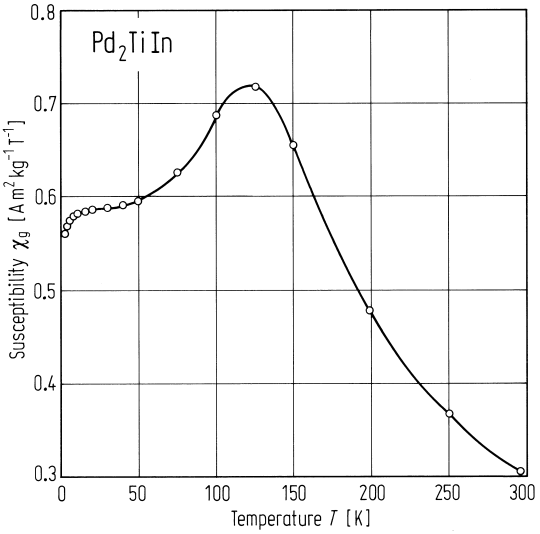

Fig. 128. Magnetic susceptibility of Pd_2TiIn as a function of temperature [93N2].

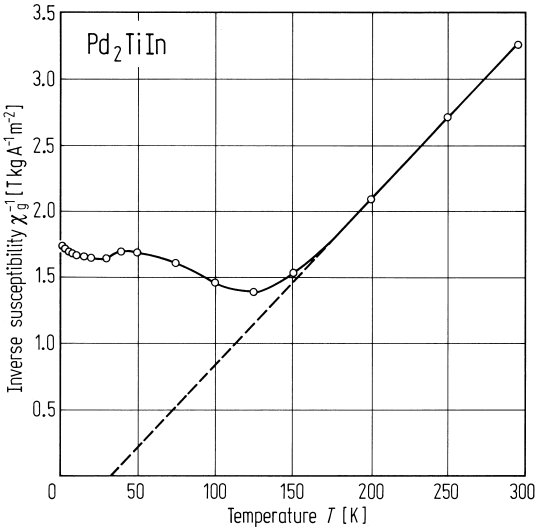

Fig. 129. Inverse magnetic susceptibility of Pd_2TiIn as a function of temperature [93N2].

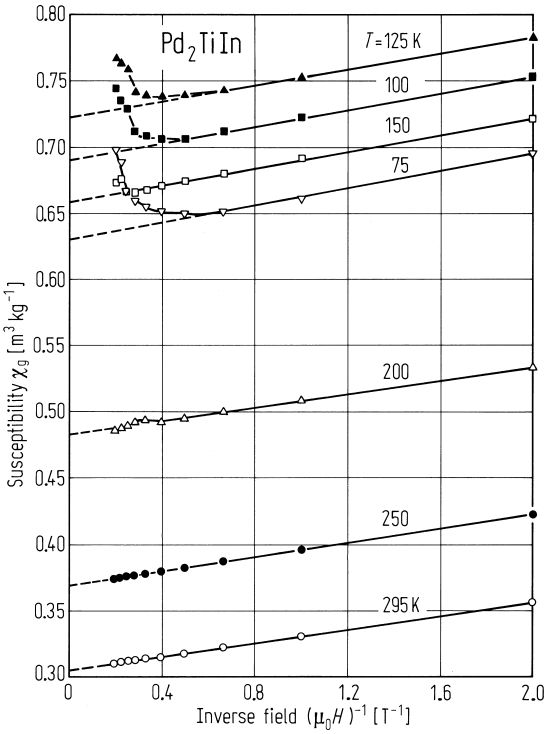

Fig. 130. Measured susceptibility as a function of the inverse applied field for a series of magnetic isotherms between 75 and 295 K. The extrapolated values give the true susceptibility of Pd_2TiIn and the gradient of the isotherms enables the magnetisation of the impurity to be determined. It may be seen that the gradient does not effectively change as a function of temperature, indicating that the Curie temperature associated with the impurity is far above room temperature. As the temperature decreases the isotherms are no longer linear over the entire range of fields employed, but there is a tendency for the susceptibility to increase for the highest field values. This suggests a transition to a higher state of magnetisation [93N2].

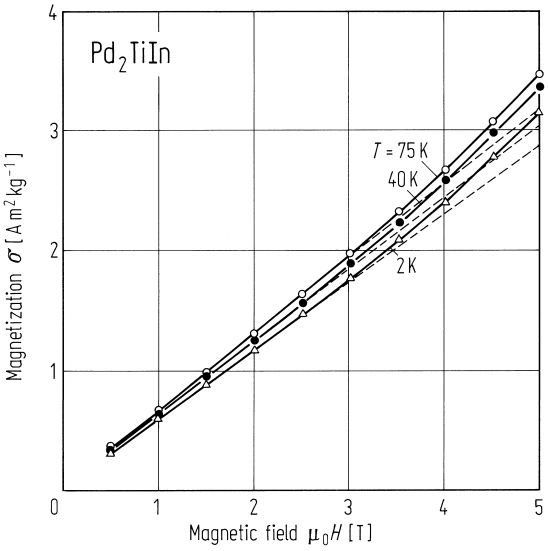

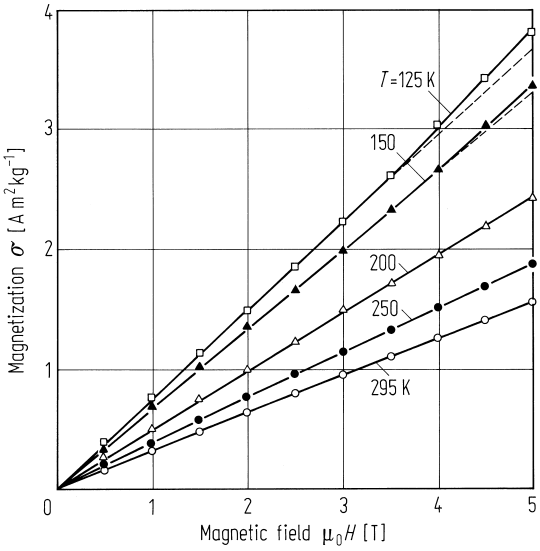

Fig. 131. Magnetic isotherms showing the magnetisation as a function of applied field. It may be seen that for the highest temperatures the isotherms are accurately linear, but as the temperature decreases there is a tendency for the magnetisation to increase for fields approximately greater than 3 T [93N2].

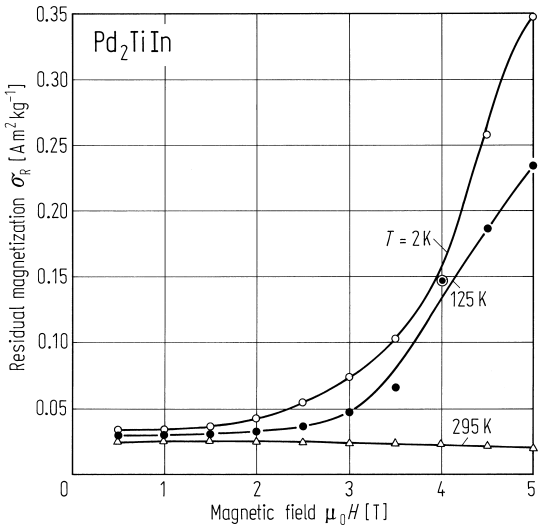

Fig. 132. Residual magnetisation σ, additional to the purely magnetic component, as a function of magnetic field. The highest values of σ_R correspond to a moment of 0.003 μ_B per formula unit [93N2].

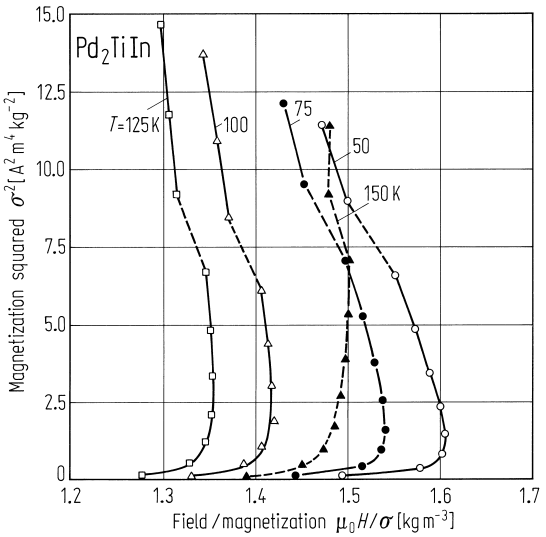

Fig. 133. Arrott plots for Pd_2TiIn [94O1].

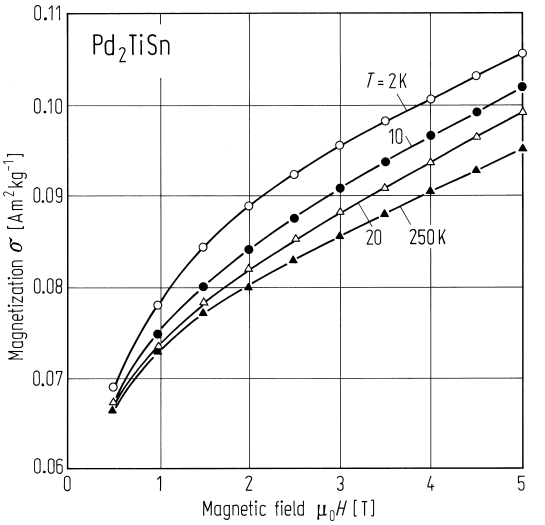

Fig. 134. Magnetic isothermals of Pd_2TiSn as a function of applied magnetic field [95N1].

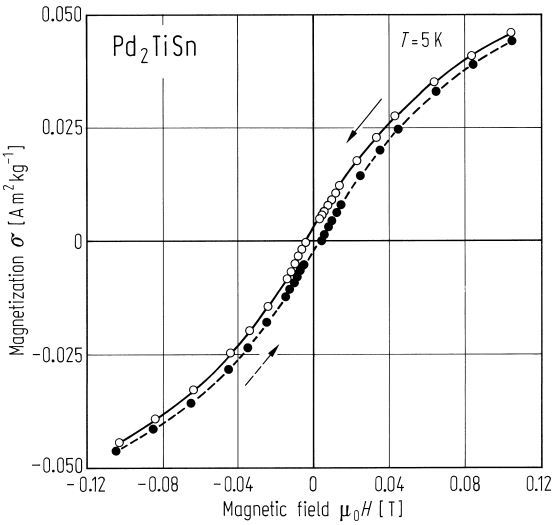

Fig. 135. Magnetic hysteresis of the Pd_2TiSn at 5 K [95N1].

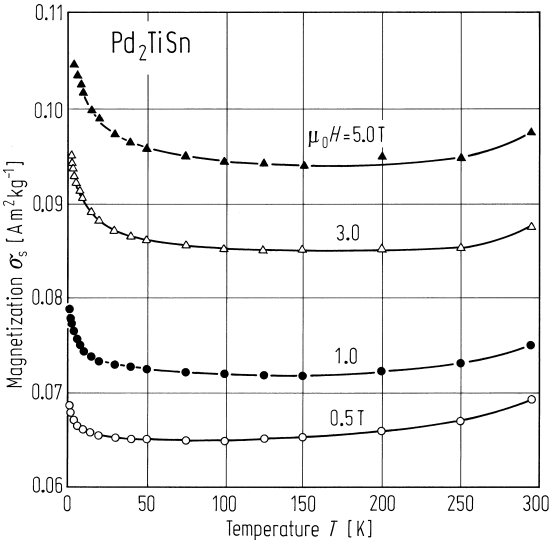

Fig. 136. Spontaneous magnetisation of Pd_2TiSn as a function of temperature [95N1].

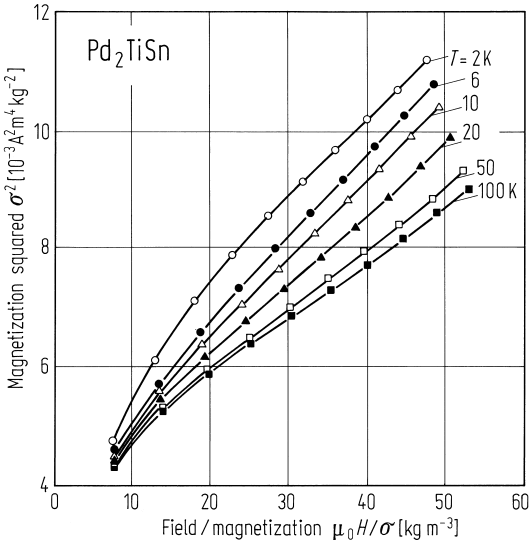

Fig. 137. Arrott plots for Pd_2TiSn showing isotherms below 295 K. It may be seen that the high field parts of the isotherms appear to converge to a single point close to the σ^2 axis. Furthermore the gradient does not appear to significantly change with temperature over the range of measurements [95N1].

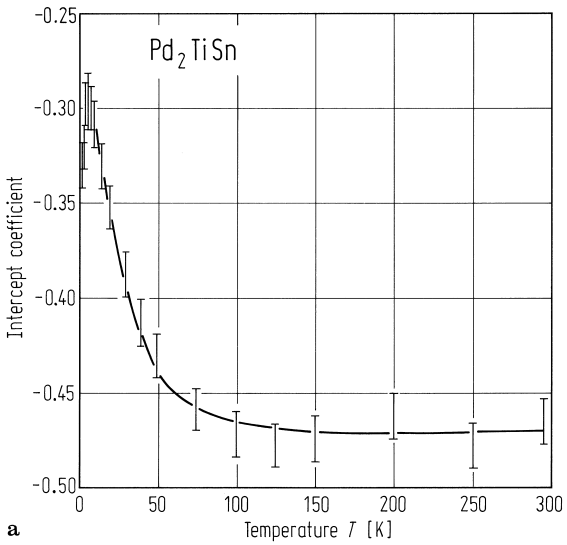

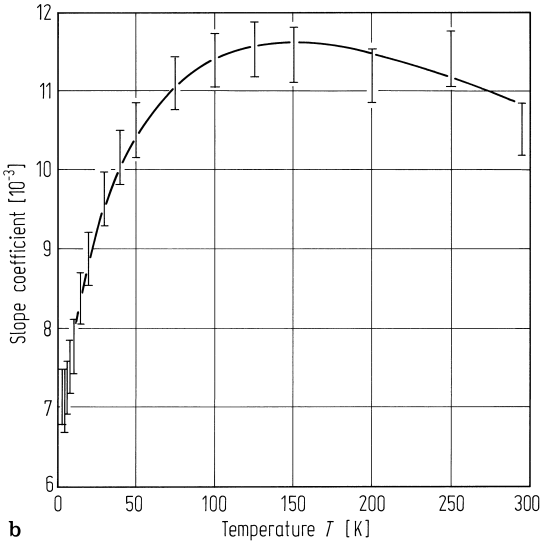

Fig. 138. (**a**) Variation of the extrapolated intercept of the Arrott plots as a function of temperature. (**b**) Thermal variation of the gradient of the isotherms in the Arrott plots for Pd_2TiSn [95N1].

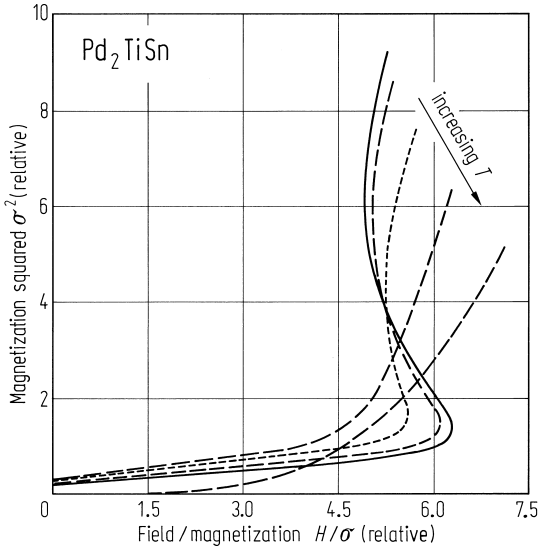

Fig. 139. Arrott plot of a system comprising two coupled paramagnetic systems $\sigma_{tot} = \Sigma + \sigma$, with coupling between them. The lower parts of the isotherms shown in the figure are for a system in which the coupling constant is much stronger than the applied magnetic field. For such a case, the isotherms converge onto the M^2 axis (see Fig. 131 above). Arbitrary units have been used for both axes [95N1].

Model

Landau theory has been used to interpret these data.

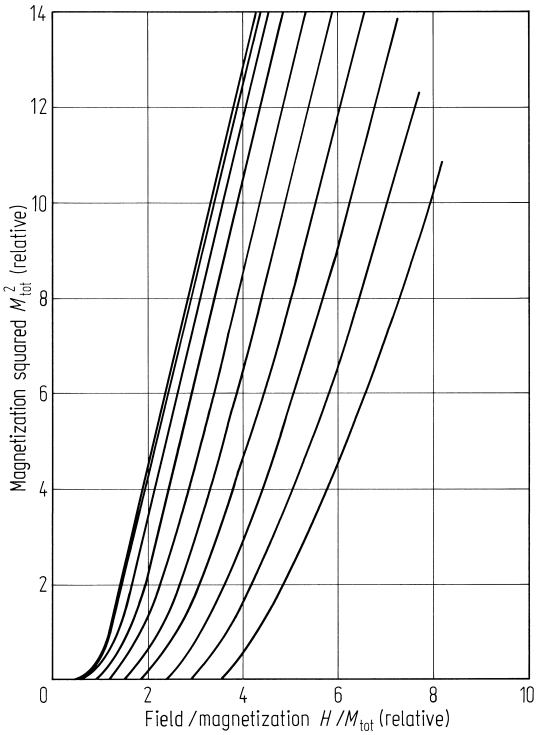

Fig. 140. Arrott plot of a system which comprises two coupled paramagnetic subsystems with $M_{tot} = M + m$. The temperature is varied over a wide interval, with the intersection with the x-axis (as determined by the inverse Pauli paramagnetic susceptibility) indicating the range over which the temperature is varied. The coupling constant C is small and taken to be 1/10th of the value used in the calculation of Fig. 141 [94N2].

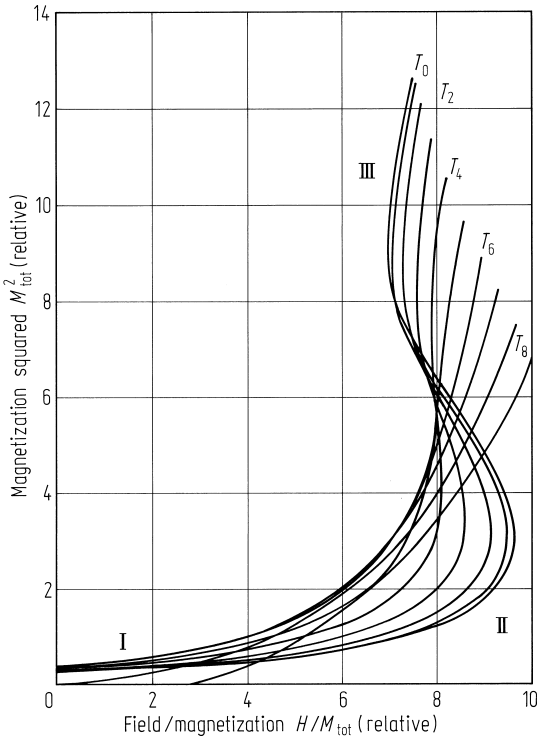

Fig. 141. Arrott plot for two paramagnetic systems and as a function of temperature with the coupling constant C large. Regions I, II and III correspond to external magnetic field much smaller than, approximately equal to and much larger than the internal magnetic field. Due to the increase of the internal magnetic field, part of the Arrott plots are displaced by a constant amount with respect to the ones in Fig. 140. For the numerical calculation the following values have been used: a_0 = 2.33, $\overline{a}$ = 0.02796, b = 3.0, A_0 = 0.51, $\overline{A}$ = 0.00408, B = 1.2, C = 8. The temperature is varied from T_0 = 0 to T_9 = 28.8 with an increase of ΔT = 3.2 in arbitrary energy units [94N2].

X_2YZ X = 3d, Y = 5f

X = 8A: Ni
Y = 5A: U
Z = 4B: Sn

Ni_2USn

AC susceptibility measurements have been used to investigate the structural phase transition.

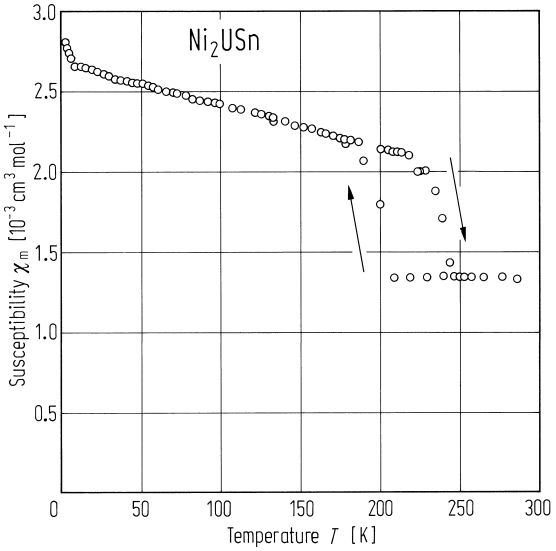

Fig. 142. DC susceptibility χ_m vs. temperature for Ni_2USn measured in a field of $\mu_0 H$ = 2 T. The discontinuity around 220 K arises from a structural phase transition [90E1].